Simulation and Validation of UNDEX Phenomena Relating to Axisymmetric Structures

R Boyd
Altair Engineering Ltd,
East Tithe, Pury Hill, Nr. Alderton, Northants, NN12 7TB, UK.
Tel: +44 (0) 1327 810713
Email: boyd@altair.com

R Royles
Department of Civil and Environmental Engineering,
Crew Building, West Mains Road, University of Edinburgh, Edinburgh, EH9 3JN, UK.
Tel: +44 (0) 131 6505732
Email: r.royles@ed.ac.uk

K M M El-Deeb
Linear & Non-linear Structural Dynamics Ltd,
182/5 Granton Road, Edinburgh, EH5 1AJ, UK.
Tel: +44 (0) 131 5395810

Abbreviations:

ALE	- Arbitrary Lagrangian-Eulerian
FE	- Finite element
FSI	- Fluid-structure interaction
GRP	- Glass reinforced plastic
JWL	- Jones Wilkins Lee
LNG	- Liquefied natural gas
MMALE	- Multi-material ALE
RPT	- Rapid phase transition
SPC	- Single point constraint
UNDEX	- Underwater explosion

Keywords:
Arbitrary Lagrangian-Eulerian, fluid-structure interaction, multi-material Eulerian, rapid phase transition, UNDEX

ABSTRACT

Numerical modelling of underwater explosion (UNDEX) loading using LS-DYNA was studied in free field conditions and in relation to an axisymmetric thin shell of revolution - an echinodome in a floating submerged and tethered configuration. The formulation utilised was multi-material arbitrary Lagrangian Eulerian. Based on preliminary modelling, backed by existing data, numerically reproducible experiments were designed for validation purposes. The mesh generation and experimental validation are described and compared.

INTRODUCTION

Offshore structures located in the submerged environment operate in more attractive conditions than at the surface. Such less demanding conditions allow for transport and storage of resources to be more continuous. Examples of submerged structures include pipelines, submarines and underwater storage tanks.

However, such structures are at risk from loading due to fast transient dynamic events, underwater explosion (UNDEX) loading. When a structure is in the vicinity of such an event the processes involved become problem dependent and often require repeated studies to establish adequate design criteria to ensure structural integrity and gain sufficient understanding of complex structural response.

Research into computational techniques, in particular the finite element method, to assist in the study of UNDEX phenomena has led to the development of general purpose codes, hydrocodes (Mair 1996).

This paper reports on the utilisation of the finite element (FE) method to design experimental UNDEX studies, a description of experimental UNDEX studies performed on a prototype structure without invoking structural damage and the numerical simulation of the experimental studies using LS-DYNA (a hydrocode) to predict fluid and structural responses.

APPROACH

The Echinodome

Much work has been done on examining the optimum shape for underwater storage tanks (Royles 1980, Sofoluwe 1980). This work concluded that a spheroidal shell, the echinodome, based on the membrane theory for thin shells, was an ideal shape for the most efficient use of material. The meridional profile of the shell is determined by the pressure head at the apex, z_o, and material strength parameter (design stress $\times$ thickness), $\sigma_d t$.

The design of a full-scale echinodome to be used for the storage of liquefied natural gas (LNG) was investigated (El-Deeb 1990), based on an earlier proposal (Royles 1984). LNG is a hazardous commodity stored either under high pressure or at very low temperatures, or a combination of both. However, in the event of leakage of LNG into the seawater caused by structural failure, a rapid change of state would occur from liquid form back to gas. Such a phenomenon is known as a rapid phase transition (RPT) and the speed with which this change of state occurs resembles the detonation of an explosive charge underwater.

The RPT would destroy the structure from which the leakage occurred. The sudden release of energy would create a compression or shock wave propagating outwards from the source to neighbouring structures, similar to underwater explosion (UNDEX) loading. The period of such loading is initially of the order of microseconds increasing to milliseconds as the shock wave propagates outwards.

Underwater Explosions
The physical characteristics of an UNDEX event have been well established (Cole 1948) and can be used to describe the processes occurring in an RPT event.

The foundations for utilising LS-DYNA to simulate UNDEX loading have been established earlier (Boyd 1997, Boyd 1999). LS-DYNA's ability to model detonation, shock wave propagation and free field fluid response using the multi-material Eulerian capabilities were successfully validated against theoretical and experimental results. A suitable discretisation for the echinodome response to hydrostatic effects was also established (Royles 1996).

Design of Experiments
A study of fluid and structural response predictions to UNDEX loading was undertaken, prior to performing experiments on an existing prototype echinodome, to assist in their design such that measurable results would be produced whilst minimising the damage to the shell. Previously undertaken experiments and numerical comparisons have been reported elsewhere (Boyd 1998, El-Deeb 1999).

The experiments were designed to consider two directions of UNDEX loading on the shell, axisymmetric and symmetric. Only the axisymmetric load case required modelling to provide sufficient data for the choice of a suitable charge mass for all load cases, since it was likely to induce the severest loading.

The experiments, and thus the numerical model, comprise three main components: the test tank (and entrained fluid), the prototype shell and the charge. The experiments are described in more detail elsewhere (Boyd 1999).

Test tank
The geometry of the test tank, and shell and charge locations are illustrated in figure 1. Using axisymmetry a 22.5^{o} wedge model was eventually adopted, reducing the pre-processing time and computational cost of the numerical model considerably. The vertical symmetry planes acted in the same manner as reflecting boundaries where fluid is assumed not to flow normal to the boundary, only along it. In order to avoid modelling the materials used in the walls and floor of the tank they were assumed perfectly rigid acting as reflective boundaries. Reflections from rigid boundaries might serve to augment the pressure at a particular location. The platform and walkway were not required to be modelled.

Prototype shell
The axisymmetric structure used in this work was a glass reinforced plastic (GRP) echinodome (Royles 1980). Geometric and material characteristics for the shell are summarised in tables 1 and 2. The pressure head for which the shell was designed (1.525m) dictated the depth of the charge and shell, and the position of the shell relative to the tank walls. The seam of the shell lay perpendicular to the longitudinal centreline of the tank, however, the numerical model assumed the shell to be monolithic. The shell was to be empty throughout the duration of the experiments. In the numerical model, the ropes tethering the shell to the tank floor were not modelled. The structure was assumed to be neutrally buoyant, but gravity was included to model the hydrostatic pressure on the shell, although the initial stress due to hydrostatic pressure was found earlier to invoke negligible stresses on the shell (El-Deeb 1990). The atmospheric pressure was ignored. Imperfections in the shell were included in the form of circumferential variations in thickness only.

Table 1. Geometric characteristics of the echinodome

Component	Dimension	Value(mm)
tufnol base	B	200
max. shell dia.	D	450
shell base dia.	D_b	170
max. shell height	H	380
total water depth	H_w	3470
tufnol base thickness	t_b	20
shell wall thickness	t_w	3.8
design head	z_o	1525

Figure 2 details the strain and pressure gauge positions for the prototype shell throughout the experiments. These positions determined which shell and brick elements' output should be requested to predict the structural and fluid responses.

Table 2. Material characteristics of the echinodome

Property	Value
Shell wall (GRP)	
Ultimate tensile strength	55.4 MPa
Young's modulus, E	8800 MPa
Poissons ratio, ν	0.36
Mass density, ρ	1100 kgm^{-3}
Shell base (tufnol)	
Young's modulus, E_b	13200 MPa
Poissons ratio, ν_o	0.284
Mass density, ρ_o	1360kgm^{-3}

Charge

The axisymmetric UNDEX loading was to be applied by placing an explosive charge 1.0m directly above the apex of the shell. A model of a cylindrical 10g charge of EDC-1 explosive material, with a height to diameter ratio equal to unity, was initially used to provide the loading. The estimation of this charge size was based on the static material failure strain (-6295$\mu\varepsilon$), tension +ve. Details of the calculation are reported elsewhere (Boyd 1999).

A sketch of the geometry of the adopted FE model is depicted in Figure 3. The discretisation is shown in Figure 4. Arbitrary Lagrangian-Eulerian (ALE) smoothing was permitted in each region of fluid which had nodes coincident with the Lagrangian elements of the shell model. Flow normal to the free surface was defined using single point constraints (SPCs) to permit any cavitation. At the air-water interface (free surface) reflections of negative pressure could be initiated leading to cavitation effects which could have serious repercussions on proximate structures. The fluid region was meshed with a total of 81628 multi-material Eulerian brick elements, and modelled using the Gruneisen equation of state (equation (1)) with the constants given in table 3. The 10g charge was meshed using 10 multi-material Eulerian brick elements and modelled using the Jones Wilkins Lee (JWL) equation of state (equation (2)). The JWL constants for EDC-1 are given in Table 4. The number of fluid elements next to the shell governed the number of elements representing the shell. Using the ALE coupling technique, 93 Belytschko-Lin-Tsay Lagrangian shell elements were tied to the fluid elements.

Table 3. Properties and Gruneisen constants of water

Symbol	Property	Water value
ρ_o	density	1000 kgm^{-3}
c	speed of sound	1484 ms^{-1}
S_1	material constant	1.979
S_2	"	0.0
S_3	"	0.0
γ_o	"	0.11
a	"	3.0
E_0	initial internal energy	3.072×10^5 Jkg^{-1}
V_0	initial relative volume	1.0

$$P = \frac{\rho_o c^2 \mu \left[1 + \left(1 - \frac{\gamma_o}{2} \right) \mu - \frac{\alpha}{2} \mu^2 \right]}{\left[1 - (S_1 - 1)\mu - S_2 \frac{\mu^2}{\mu + 1} - S_3 \frac{\mu^3}{\mu + 1} \right]^2} + (\gamma_o + a\mu) E_1 \qquad (1)$$

$$P = A\left(1 - \frac{\omega}{R_1 V} \right) e^{-R_1 V} + B\left(1 - \frac{\omega}{R_2 V} \right) e^{-R_2 V} + \frac{\omega E_1}{V} \qquad (2)$$

where $E_1 = E_o/\rho$ and V represents the volume of exploded material.

Table 4. Properties and JWL constants of explosive material EDC-1 (Didham 1992)

Symbol	Property	EDC-1 value
ρ	density	1795 kgm^{-3}
D	detonation velocity	8716 ms^{-1}
P_{cj}	Chapman-Jouget	34.25×10^9 Pa
A	material constant	9.036×10^{11} Pa
B	"	9.033×10^9Pa
R_1	"	4.647
R_2	"	0.8717
ω	"	0.275
E_0	initial internal energy	$1.050\times10^{10}$$Jkg^{-1}$
V_0	initial relative volume	1.0

To minimise computation time, it was assumed at this stage that the shock pulse would generate the highest strains on the structure. Hence fluid and structural responses for the first 5.0ms only were of interest - enough time for the shock wave to completely engulf the structure, but insufficient time to allow interference by boundary reflections. Earlier findings (Boyd 1999) concluded the Donor cell & HIS advection scheme to be the most computationally efficient for a free field UNDEX problem and, consequently, this was utilised for initial fluid-structure interaction (FSI) simulations.

DISCUSSION OF RESULTS

Initial results

From all positions the highest predicted peak strain was almost 80% of the static material failure strain (-6295με). These levels were considered in danger of invoking material non-linearity.

Based on the predicted responses obtained, it was decided to reduce the charge size to 5g in the experimental axisymmetric load case in order to avoid any risk of damage to the structure.

Experimental DATA

The general arrangements (Boyd 1999) for the test tank, shell and charge for the axisymmetric load case were as depicted in Figures 1and 2. Structural response was measured using rectangular strain gauge rosettes bonded to the outer surface of the shell according to figure 2. The gauges to be located on the seam were offset by 10mm to ensure the measured response was that of the GRP material and not of the seam. Pressure in the fluid was measured using tourmaline gauges. The free field gauges were suspended from steel bars at the charge depth for each load case. The recording frequencies were 100kHz for strain gauges and 1MHz for pressure gauges.

Typical fluid responses are displayed in Figures 5(a)-(c). The free field fluid responses (Figure 5(a)) were measured 1.0m off to the side of the charge (1.0m standoff). The arrival of the shock front is identified by a rapid increase in pressure to a peak value of 4.325MPa followed by a rapid exponential decay. The pressure is then observed to increase 45ms after the initial shock pulse, indicating the arrival of the first bubble pulse. Table 5 compares the parameters relating to the shock and first bubble pulses at two gauges, 1.0m standoff from 5g EDC-1. A second bubble pulse was detected at 79ms.

Table 5. Comparison of shock wave and first bubble pulse characteristics at 1.0m standoff from 5g EDC-1

Gauge No.	Peak pressure (MPa)		Impulse, I (Pa.s)		Energy, E_f (Pa.m)	
	Shock	Bubble	Shock	Bubble	Shock	Bubble
8	4.081	0.699	189.61	160.95	124.35	23.84
9	4.325	0.694	186.49	168.02	121.38	24.13

The fluid response close to the shell is depicted for the positions $\phi = 0^o$, $\theta = 0^o$ (the apex) and $\phi = 90^o$, $\theta = 0^o$, (the maximum diameter) in Figures 5(b) and (c) respectively. At the apex, the fluid response is characterized by a sharp rise followed by a rapid decay to negative pressures, possibly indicating cavitation. The total pressure peak is observed to be approximately 20% higher than that recorded at the free field gauges which indicates reflected pressures from the surface of the shell. At the maximum diameter an initial gradual form of loading with several sharp peaks is observed. The duration of this loading was such that it would appear to the prototype shell as an application of quasi-static load on the maximum diameter for a period of almost 1.0ms. It appears as though significant cavitation was occurring after the arrival of the shock wave, however, the pressure gauges were unable to quantify cavitation. The negative pressures recorded here were below absolute zero (-0.1MPa) which is physically impossible. The data does however, strongly indicate that cavitation was occurring.

A strain-time history for the apex position is depicted in Figure 6 and is seen to exhibit a rise in initial peak response, reducing prior to peak response. The significance of the first bubble

pulse at 45ms is again clearly evident. The severity of the bubble pulse loading generated strain rates and peak strains higher than the initial shock pulse.

At no position did the initial or secondary peak strains exceed the maximum allowable strain of the GRP material (-6295με) under axisymmetric loading conditions. The highest peak strain recorded, in the apex region, came to within 53% of the ultimate value.

Validation of Numerical Simulations

Poor results from earlier simulations performed in modelling the bubble pulse in the free field environment (Boyd 1999) reduced confidence in using the multi-material Euler technique for predicting bubble loading on the shell, and consequently it was decided not to run a simulation to bubble time with this technique. A simulation time of 5.0ms was thus chosen to capture the FSI due to the shock pulse only.

The numerical model described earlier was modified to incorporate a 5g EDC-1 charge. Each of the four advection schemes available in LS-DYNA (Anon. 1997) was examined for accuracy and computational cost. The results are listed in table 6. All schemes were observed to underpredict the peak pressure by approximately 20% on average. The second order van Leer advection scheme was closest to the experimental values.

Table 6. Comparison of MMALE predicted peak pressures for various advection schemes under 5g EDC-1 at 1.0m standoff (axisymmetric), 22.5^0 wedge model

Advection Scheme	Free field Pressure (MPa)	Total pressure at $\phi = 0^o$ (MPa)	Solution time (s)
Donor cell	3.28	2.92	68979
van Leer & HIS	3.16	2.54	125225
van Leer	3.38	3.09	94375
Donor cell & HIS	3.08	2.78	70677

The pressure-time history predicted by the MMALE axisymmetric model using the van Leer scheme is compared with the experimentally measured pressure record and predicted results from preliminary work on a one eighth sphere model (Boyd 1999) in Figure 7. The experimental pressure-time curve was simulated poorly by both models. The slow rise time suggests the discontinuity at the shock front is smeared over a number of elements, the aspect ratio of which is poor (≈ 1.5) in the direction of propagation (1.0m to the side of the charge). The smearing of the shock front consequently reduces the peak pressure. Also, the small number of elements in the charge may not have permitted the full build-up to detonation pressure, as was concluded necessary from earlier work (Boyd 1999). Due to the small element sizes involved, to use a sufficient numbers of elements would have been impractical.

The predicted pressure decay behind the shock front consists of several oscillations of decreasing amplitude, as was observed with 10g EDC-1 and a one eighth sphere model (Boyd 1999). It is noteworthy however, that the measured decay appears to correspond with the mean values of oscillations. If a finer mesh were used the correlation of the predicted and measured decays might improve.

The pressure record from the one eighth sphere model, Figure 7, although an improvement over the pseudo-wedge model, is observed to overpredict the measured peak pressure by approximately 20%. This result is higher than the pseudo-wedge model and could be expected, as the discretisation in the direction of propagation was significantly finer.

The MMALE predicted physical propagation of the shock wave around the shell is illustrated in figure 8(a) - (d). The shock wave maintains its sphericity as it engulfs the shell, and the shock front is well defined whilst in the vicinity of the shell. Diffraction of the shock front is observed, manifested by reduced pressure, close to the surface of the shell. Later in time scattered pressures from the apex and base of the shell are seen after the shock wave has passed. Elsewhere the shock front is noticeably smeared, particularly in the region of the mesh off to the side of the charge.

Table 7 lists the predicted total pressure peaks at various positions around the shell and compares them with the experimental values. Figure 9 depicts a typical total fluid pressure response at the maximum diameter of the shell ($\phi = 90^o$, $\theta = 0^o$) predicted using the van Leer advection scheme. The prediction of the general trend of the pressure response over the first millisecond was encouraging and the longer duration pulse at $\phi = 90^o$ was clearly simulated. However, all pressure-time histories were observed to suffer excessively from noise and at all positions the peak pressure was underpredicted.

Table 7. Comparison of experimental and MMALE predicted peak total pressures under 5g EDC-1 at 1.0m standoff (axisymmetric)

Position ϕ, θ	Experimental pressure (MPa)	Predicted pressure(MPa)	% difference
0^o,0^o	5.320	3.09	-42%
45^o, 0^o	3.630	1.62	-55%
90^o, 0^o	0.813	0.67	-18%
135^o, 0^o	1.678	1.05	-37%

A comparison of measured and predicted shell response at $\phi = 0^o$, $\theta = 0^0$ and $\phi = 150^o$, $\theta = 0^0$, for the meridional and circumferential directions respectively, is presented in figures 10(a) and (b).

Table 8. Comparison of experimental and MMALE predicted initial peak strains under 5g EDC-1 at 1.0m standoff (axisymmetric)

Position ϕ, θ	Initial peak strain ($\times 10^6$)			
	Circum.		Merid.	
	Expt	MMALE	Expt	MMALE
0^o,0^o	-3164	-1955	-2368	-3696
30^o, 0^o	-1766	-1871	-2123	-1731
60^o, 0^o	-997	-1349	-754	-1337
90^o, 0^o	-1224	-741	-1003	-1451
120^o, 0^o	-1034	-1080	-926	-1877
150^o, 0^o	-1833	-1250	-1439	-2347

Qualitatively, the general trend at $\phi = 0^o$ over the first millisecond is well reproduced, suggesting the simulated shell behaviour associated with the UNDEX loading is in good agreement with the experimentally observed behaviour. Over 5.0ms the predicted signal is observed to exhibit the initial peak and decaying response that the measured signals possess. This is an indication of the damping effect of the inertia of the surrounding fluid. Also, as observed experimentally, the rise to the initial peak at the apex features a small reduction in strain prior to peak response. The highest strain recorded experimentally at $\phi = 150^o$ was in

the meridional direction. However, the predicted results are in poor agreement with this situation, the peak strain occurring in the circumferential direction, see Table 8.

The overpredicted shell response does not necessarily render the MMALE technique incapable of being utilised to make dynamic buckling load predictions. The MMALE technique provides a good representation of the physics of an UNDEX event and generates an approximate loading for the desired charge size at a given standoff distance. The fact that the strains were generally overpredicted implies a conservative estimate could be obtained to determine at what load failure would occur geometrically, and to compare with the load required to invoke material failure.

CONCLUSIONS

1. The predicted physical propagation of the shock wave up to and around the shell was in good agreement with previous observations.

2. The quality of the pressure-time history associated with the shock wave at the standoff point is in question, being characterized by a series of slow rising oscillations of decreasing amplitude at the free field position. The peak pressure is within 10% of the measured experimental value.

3. The fluid response at the shell was underpredicted compared with experimental measurements and found to be less than the incident pressure at the apex.

4. The sequence of peak strains down the $\theta = 0^o$ meridian is well reproduced. However, the direction in which the experimental peak strains were found to occur was not replicated.

5. The predicted response of the shell was found generally to be overpredicted compared with the experimental results. However, the highest strains did coincide with the critical regions observed experimentally.

The van Leer advection scheme is computationally the most accurate and cheapest scheme to use with the MMALE pseudo-wedge model for applying the shock loading to the shell. Given the conservative predictions of structural response from the model this approach could be used to estimate dynamic buckling criteria for UNDEX loading.

ACKNOWLEDGEMENTS

The authors are grateful for the support of DERA (Rosyth), EPSRC, Oasys Ltd and the University of Edinburgh.

REFERENCES

Anon. (1997). LS-DYNA keyword user's manual version 940. Livermore Software Technology Corporation, 97 Rickenbacker Circle, Livermore, CA 94550, USA.

BOYD, R. and ROYLES, R. (1997). "Modelling free field UNDEX using LS-DYNA3D." Proc. 1st European LS-DYNA Conference, Stratford-upon-Avon, England, UK, 18:S2.1-2.11, 20-21 March.

BOYD, R., ROYLES R., EL-DEEB K. M. M. and HAXTON R. S. (1998). "Fast dynamic transient loading of underwater structures." Proc. of 11th Int. Conf. on Experimental Mechanics., Oxford, Ed. Allison, Balkema, Rotterdam., Netherlands, Vol. 1, pp. 23-28, 24-28 August.

BOYD, R. (1999). Fluid-structure interaction under fast transient dynamic events. Ph.D. Thesis, University of Edinburgh, Scotland ,UK.

COLE, R. H. (1948). Underwater Explosions. Princeton University Press, NJ, USA.

DIDHAM, E. F. J. (1992). Final report on free field experimental and simulation studies of the IEPG PA29 standard omnidirectional charge. Memorandum 25/92 (unclassified). DERA (Fort Halstead), England, UK.

EL-DEEB, K. M. M. (1990). "Echinodome response to dynamic loading." Ph..D. Thesis, University of Edinburgh, Scotland, UK.

EL-DEEB, K. M. M. and Royles, R. (1999). "Response measurements on an echinodome subjected to explosive loading." Shock and Vibration, Vol. 6, pp. 45-57.

MAIR, H.U. (1996). "Preliminary compilation of underwater explosion benchmarks." Proc. 67th Shock and Vibration Symposium, Monterey, CA, SAVIAC, Arlington, VA, USA, Vol.1, pp. 361- 379, November.

ROYLES, R and BOYD, R. (1996). "Influence of high performance computing on analysis and design of underwater structures." XXV AIAS National Conference, and International Conference on Material Engineering, Gallipoli/Lecce, Italy, 4-7 September.

ROYLES, R. and LLAMBIAS J. M. (1984). "Storage aspects of liquid gases underwater and the structural implications." Proc. of Int. Symp. on Storage and Transport of LPG and LNG Koninklijke Vlaamse Ingenieursvereniging, Technologisch Institut (Kommissie Metaalbouw), Antwerpen, Belgium., Vol. 2, pp. 55-72.

ROYLES, R., SOFOLUWE A. B., BAIG M. M., and CURRIE A. J. (1980). "Behaviour of underwater enclosures of optimum design." Strain., Vol. 16, pp. 12-20.

SOFOLUWE, A. B. (1980). "Studies of a structural form for underwater structures." Ph..D. Thesis, University of Edinburgh, Scotland, UK.

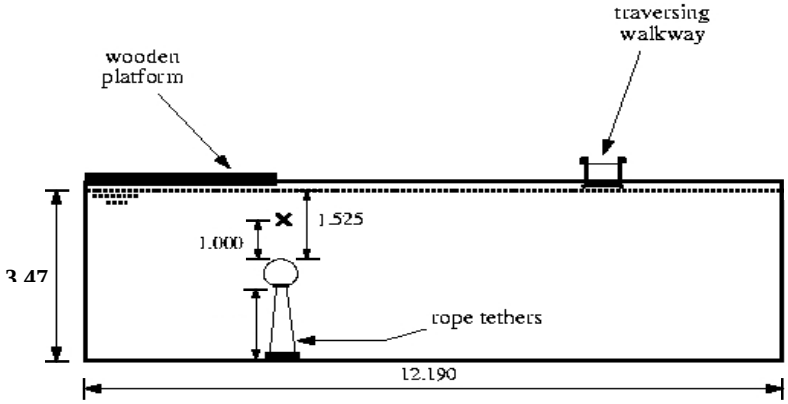

Figure 1. The test tank geometry, out of plane width = 6.090m, and shell location on longitudinal centerline (all dimensions in m)

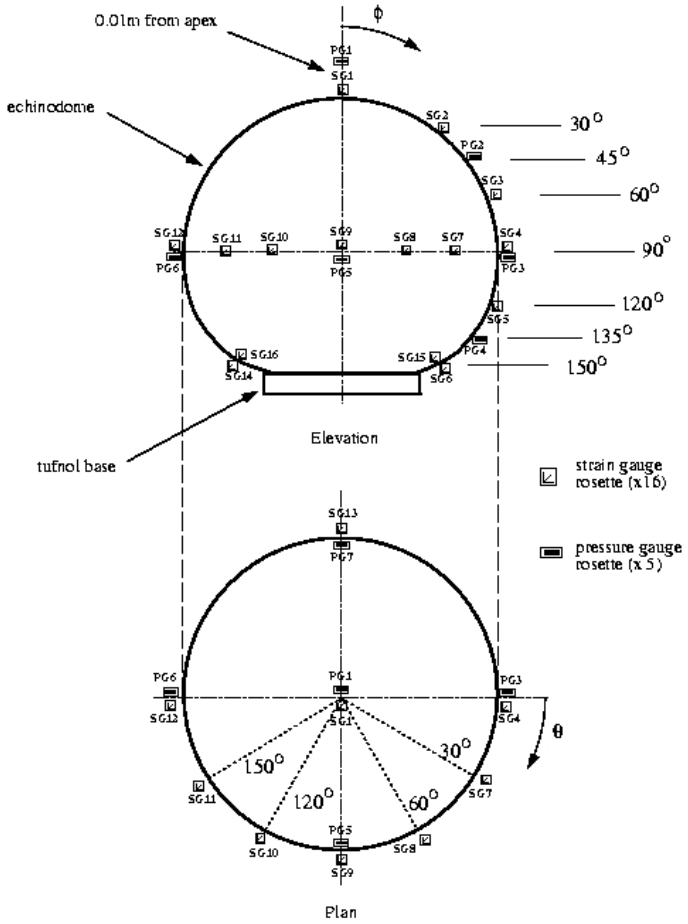

Figure 2. Prototype shell instrumentation

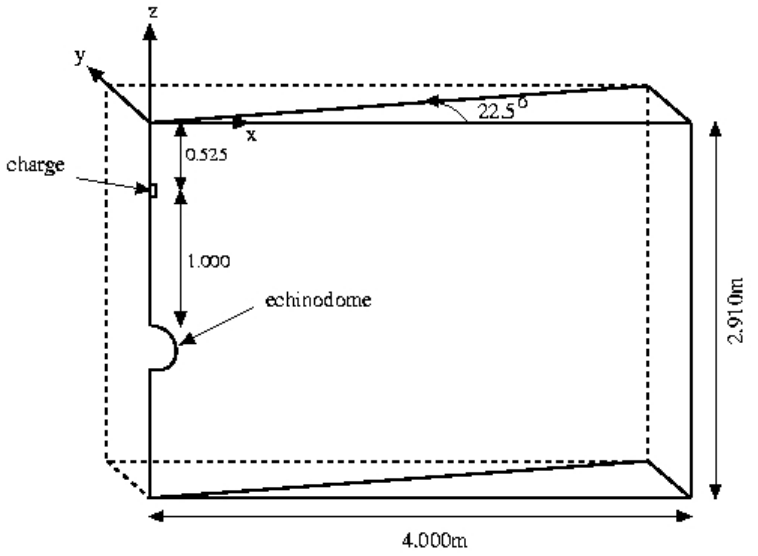

Figure 3. Sketch of pseudo-wedge model

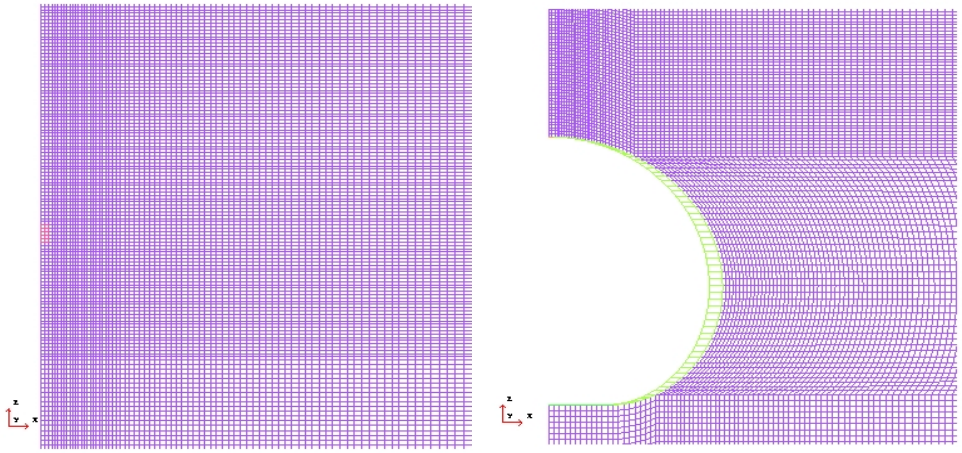

Figure 4. Finite element mesh for MMALE pseudo-wedge model

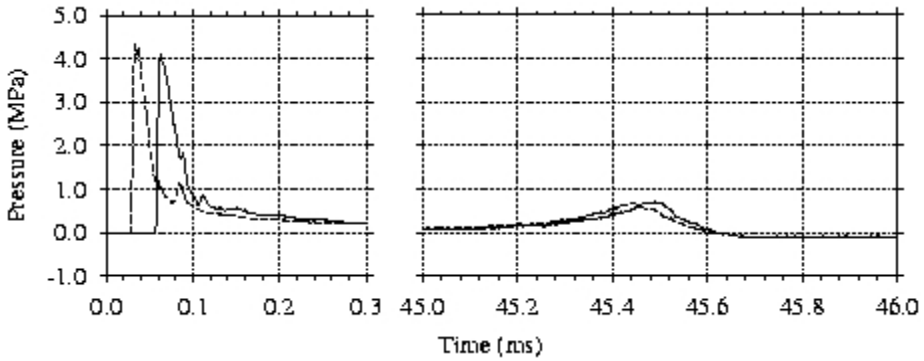

(a). Free field pressure-time history

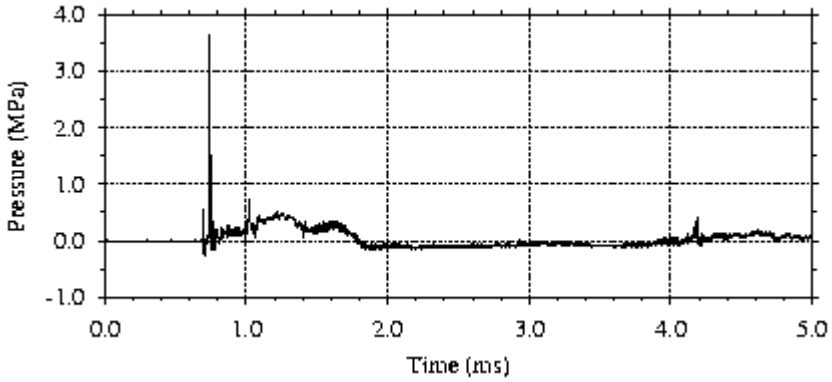

(b). Fluid response at $\phi = 0^o$, $\theta = 0^o$ on shell

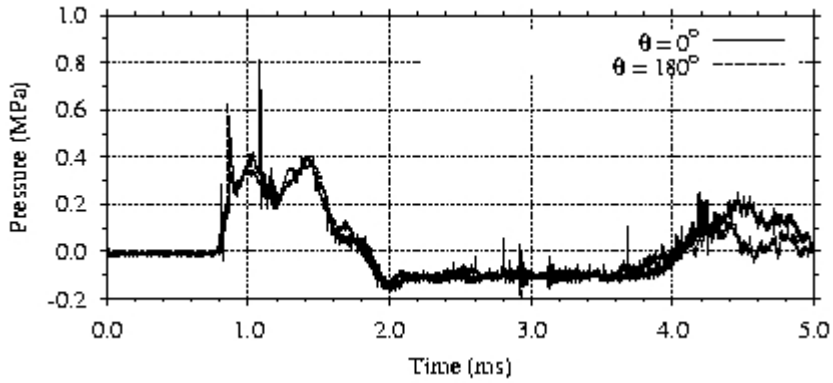

(c). Fluid response at $\phi = 90^o$, $\theta = 0^o$ on shell

Figure 5. Various experimental fluid responses to 5g EDC-1 for 1.0m standoff (axisymmetric)

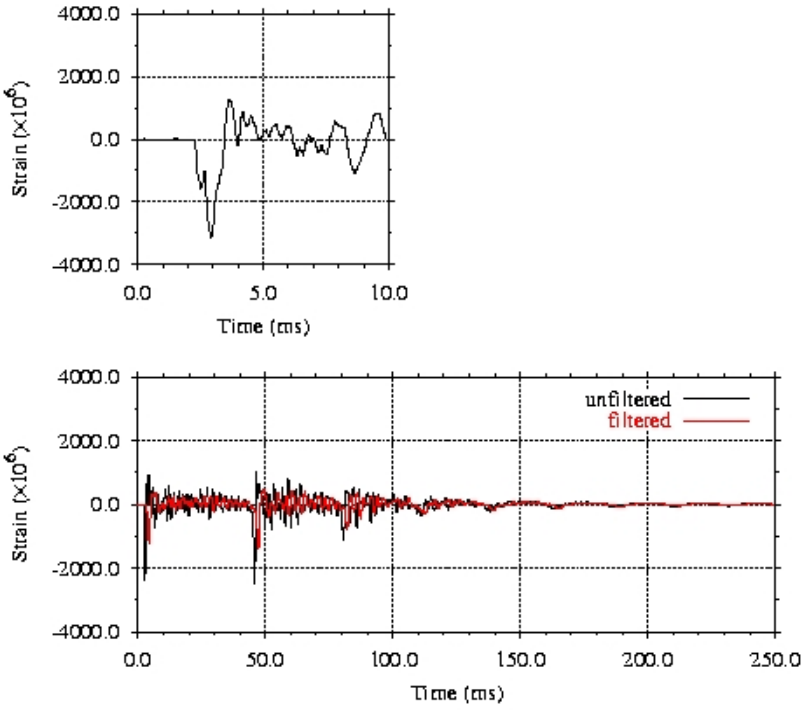

Figure 6. Circumferential experimental strain response at $\phi = 0^o$, $\theta = 0^o$ to 5g EDC-1 at 1.0m standoff (axisymmetric)

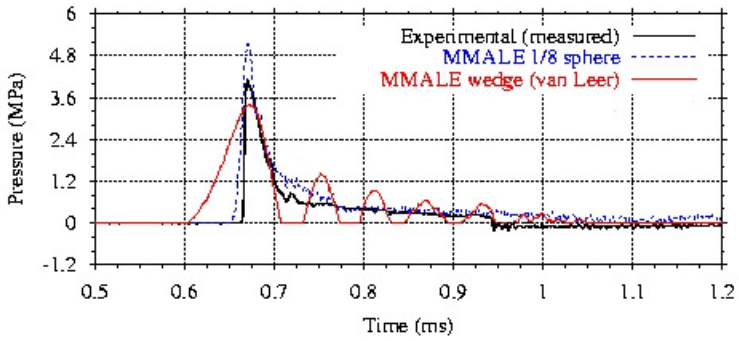

Figure 7. Comparison of free field fluid response at 1.0m standoff from 5g EDC-1

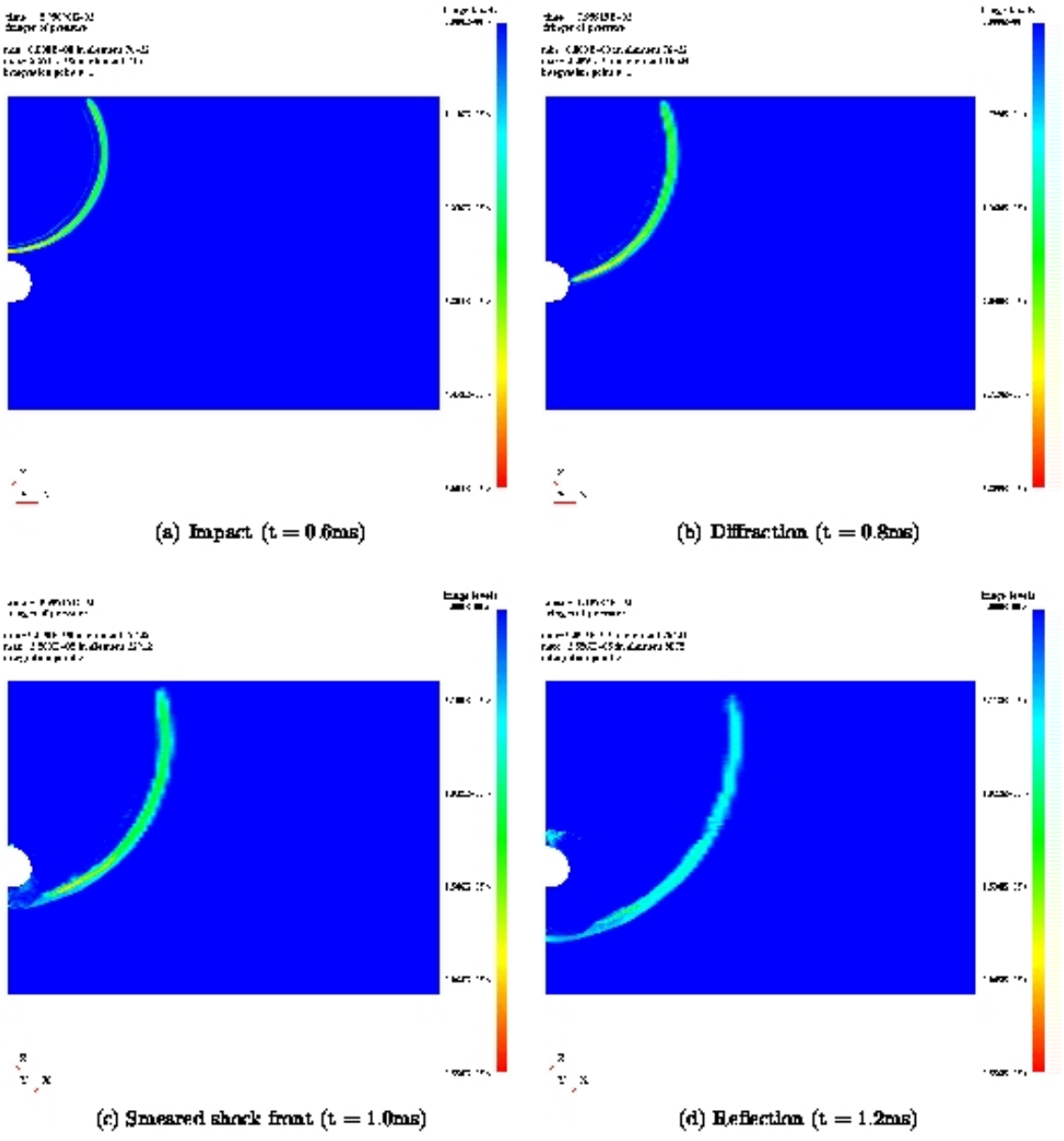

Figure 8. MMALE predicted propagation of shock wave around shell under axisymmetric loading from 5g EDC-1 at 1.0m standoff (pressure units = Pa $\times 10^{-11}$), 22.5^{o} wedge model

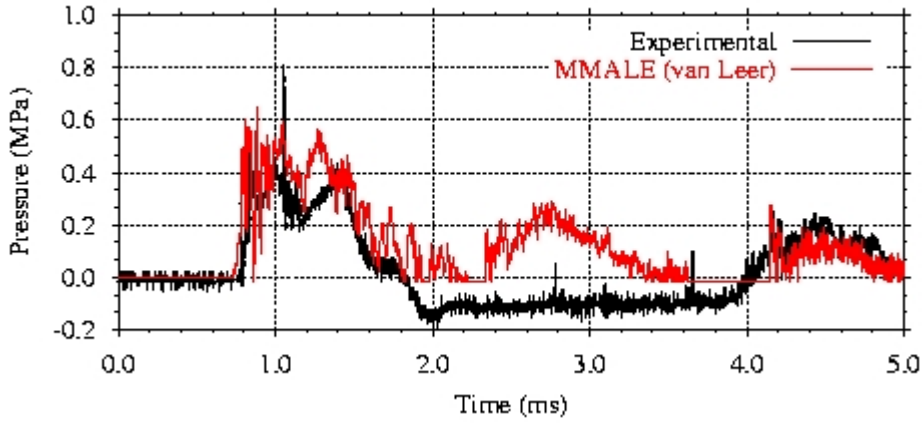

Figure 9. Comparison of MMALE predicted (22.5^o wedge model) and measured fluid response at $\phi = 0^o$, $\theta = 0^o$ to 5g EDC-1 at 1.0m standoff (axisymmetric)

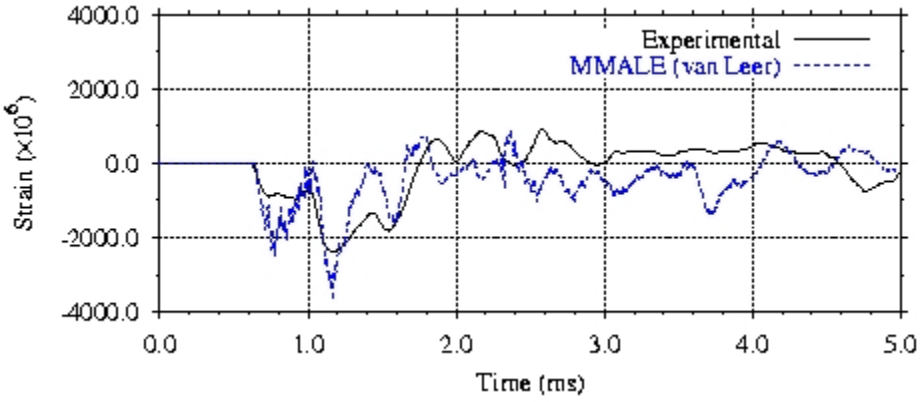

(a) $\phi = 0^o$, $\theta = 0^o$ (meridional)

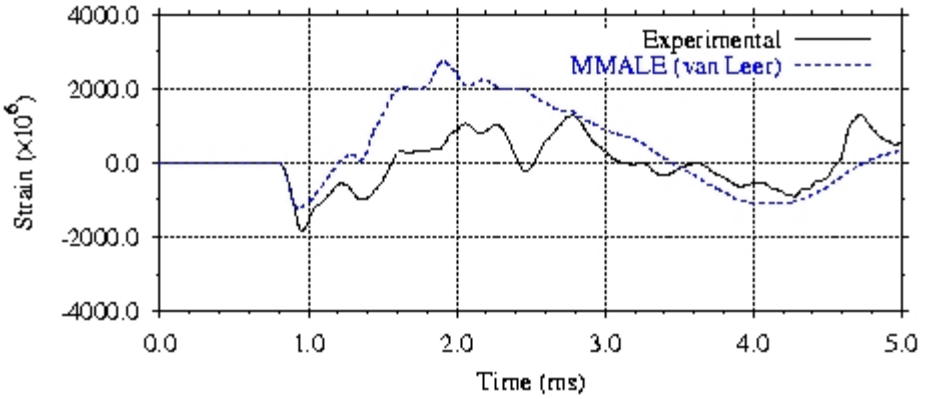

(b) $\phi = 150^o$, $\theta = 0^o$ (circumferential)

Figure 10. Comparison of MMALE predicted (22.5^o wedge model) and measured strain response to 5g EDC-1 (axisymmetric)